11-27-2012

Catalytic Studies of Sodium Hydroxide and Carbon Monoxide Reaction

Sushant Kumar
Center for the Study of Matter at Extreme Conditions, Florida International University, skuma002@fiu.edu

Vadym Drozd
Center for the Study of Matter at Extreme Conditions, Florida International University, drozdv@fiu.edu

Surendra K. Saxena
Center for the Study of Matter at Extreme Conditions, Florida International University, saxenas@fiu.edu

Article

Catalytic Studies of Sodium Hydroxide and Carbon Monoxide Reaction

Sushant Kumar *, Vadym Drozd and Surendra K. Saxena

Center for the Study of Matter at Extreme Conditions, College of Engineering and Computing, Florida International University, Miami, FL 33199, USA; E-Mails: drozdv@fiu.edu (V.D.); saxenas@fiu.edu (S.K.S.)

* Author to whom correspondence should be addressed; E-Mail: skuma002@fiu.edu; Tel.: +1-305-496-6655; Fax: +1-305-348-3070.

Abstract: We have studied the effect of ball milling on alumina mixed nickel, magnetite and Raney nickel on the reaction: $2NaOH(s) + CO\ (g) = Na_2CO_3\ (s) + H_2\ (g)$ and determined the optimum particle size for the catalysts. The best performance was shown by a 2 h ball milled Raney nickel with average crystallite size of 209 Å. This reaction serves the dual purpose of carbon sequestration and yielding hydrogen gas.

Keywords: catalyst; ball milling; crystallite size; carbon sequestration

1. Introduction

Sodium hydroxide (NaOH) has been used as a reactant to facilitate various reactions yielding hydrogen (H_2). Its inclusion in the reaction brings many advantages such as lowered operating temperature and reduced consumption of heat. We have earlier studied the interaction of NaOH with methane (CH_4), carbon monoxide (CO) and carbon(C) [1,2]. Recently, Reichman *et al.* [3] have also suggested a similar approach named ovonic renewable hydrogen (ORH). This method uses NaOH for the reformation of organic matter to produce H_2. Kamo *et al.* [4] pyrolyzed dehydrochlorinated polyvinyl chloride (PVC) and activated carbon with NaOH and steam to generate H_2 and sodium carbonate (Na_2CO_3). This process has CH_4, ethane (C_2H_6) and carbon dioxide (CO_2) as byproducts in minor percent. Onwudili and William [5] performed the hydrothermal gasification of glucose and other biomass to produce H_2. NaOH was used as a promoter in this case.

The necessity to sequester carbon emission during the production of H_2 is the main goal of this work. Once this problem is solved, various technologies are already in existence which can use H_2 as a fuel-carrier in many applications. Other than using alternate energies for electrolysis of water or the biological methods, no techniques are available to produce carbon emission free H_2 from fossil fuels. Many researchers worldwide have realized the need to produce H_2 without any CO_2 emission [1,6–14]. Carbon monoxide (CO) is a toxic gas emitted by power plants and blast furnaces with a severe impact on global warming. Generally, water-gas shift reaction uses steam to lock CO and produces CO_2 and H_2. A vast emission of anthropogenic gas (CO_2) is a major drawback of the water-gas shift reaction. We propose to solve this problem of carbon emission using a hydroxide as a reactant with CO gas [2]. One should note that the present scheme serves the dual purpose of CO capture and H_2 production.

$$2NaOH\ (s) + CO\ (g) \rightarrow Na_2CO_3(s) + H_2\ (g)\ \Delta H = -119\ kJ\ (600\ °C) \tag{1}$$
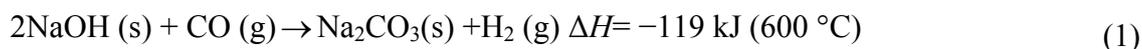
However, if NaOH is to be produced for carbonation, the method proposed here cannot be regarded as carbon-emission free because NaOH itself is produced from electrolysis of brine, which is very energy intensive process. Instead, if we use NaOH that is a byproduct from existing chlor-alkali plants, we can produce Na_2CO_3 and H_2 gas using reaction (1). Na_2CO_3 is a valuable byproduct and has many applications in chemical industries. Apart from the fact that the production of NaOH is an energy intensive process, there is also an imbalance between the global H_2 demand and NaOH production; hence reaction (1) cannot be seen as a global solution for H_2 gas. However, reaction (1) will be certainly helpful in mitigating the vast emission of greenhouse gases during production of H_2.The purpose of present work is to study the effect of catalysis on the carbonation of the hydroxide. It is highly desirable to lower the reaction time or even the operating temperature of exothermic reaction (1). Thus, we have examined several catalysts to accelerate reaction (1).

Nickel is a low cost, highly active and widely employed catalyst for industrial application [15–19]. Raney nickel catalysts possess high catalytic activity due to its highly porous microstructure and high surface area. It is extensively used in various industrial processes and also in organic synthesis process [20,21].Fe_3O_4 (magnetite) acts as a catalyst for water gas shift reaction (CO (g) + H_2O (g) $\leftrightarrow$ CO_2 (g) + H_2 (g), $\Delta H = -41.1$ kJ/mol) [22,23].

Previous results [24–26] show strong effect of the catalyst's geometric factor, electronic factor and surface imperfections. Beeck [27] correlated the catalytic activity to the lattice parameter of the contact surface. The electronic factors are dependent on the extent to which *d*-band of the crystal filled up by the electrons [28,29]. The effect of the imperfections is due to the surface imperfections (e.g., kinks, screw dislocations) which can also behave as catalytically active sites [30]. Therefore, it is important to investigate the possible relation between the catalyst grain size and the reaction rate.

In this work, different sized catalysts were prepared by mechanical milling. Mechanical milling is one of the common methods for milling powder materials to obtain uniform distribution of composition [31]. It is quite often employed due to its simplicity, low cost, and ability to form a large number of different materials [32]. During milling, powder particles experience intensive deformation which leads to various crystal defects such as lattice strains, dislocations, vacancies and morphological changes [31,33]. Here, we have studied the changes in catalysts powder morphology, average particle size and crystallite size with milling time. We also examined the relation between kinetics of reaction (1) and morphological and structural changes in the catalysts.

2. Experimental Study

2.1. Catalyst Preparation

The catalysts used in this work are alumina (Al_2O_3) mixed nickel, magnetite and Raney nickel. Nickel Powder (-100 mesh), Raney nickel (-325 mesh) and alumina were delivered by Sigma Aldrich, Acros Organics and Good Fellow respectively. The various sizes of these catalysts were obtained using planetary Retsch PM100 ball mill. The cylindrical ball milling container has internal diameter of 1.6" and internal length of 1.6". The powder to ball weight ratio was 1/54. Magnetite was ball milled for 1 and 2 h. Al_2O_3 mixed nickel was prepared in 2:1 ratio by weight. Then, this mixture was ground for 1 or 2 or 4 h. For Raney nickel, milling time was 2 and 4 h. The same revolution speed (250 rpm) was maintained for grinding all the catalyst particles.

2.2. Catalyst Characterization

X-ray diffraction patterns for different catalysts were obtained using Bruker GADDS/D8 X-ray system with Apex Smart CCD Detector and Mo direct-drive rotating anode (50 kV; 20mA). The surface morphology of the catalyst was studied using JEOL JSM-5910-LV and JEOL JSM-6330F scanning electron microscope.

Image J software was used to determine the average particle size of catalysts. A total of nearly 50 particles of each catalyst were taken into consideration from 3–4 SEM images.

2.3. Reaction Study

Anhydrous NaOH with a purity of 98% was supplied by Sigma Aldrich. About 0.10 g of NaOH was dissolved using 1 mL of distilled water in an alumina boat. Then, the catalyst (3 wt.% of NaOH) was mixed with the solution. After that, the alumina boat was placed at the hot spot position in an alumina tubular furnace (18.5" long and 0.7" in diameter). The detailed experimental set up is explained elsewhere [1].

Nitrogen (N_2) gas was allowed to flow at the rate of 50 mL/min until the required temperature was achieved. After that, N_2 flow was ceased and CO was passed through the reaction chamber at the rate of 20 mL/min.

The reaction (1) was studied at several temperatures using various sizes of the different catalysts. The extent of the reaction (1) was evaluated by calculating the amount of Na_2CO_3 formed. The method used is the titration of mixture of formed soda ash and un-reacted NaOH against 0.1009 N volumetric standard solution of nitric acid (Aldrich). The equivalents can be detected by using acid-base indicators; here phenolphthalein and methyl orange were the indicators. $NaHCO_3$ does not form in the reaction but it does during titration:

$$Na_2CO_3 + HNO_3 \rightarrow NaHCO_3 + NaNO_3 \tag{2}$$

and then

$$NaHCO_3 + HNO_3 \rightarrow NaNO_3 + CO_2 + H_2O \tag{3}$$

3. Results and Discussion

3.1. Characterization of Catalysts

3.1.1. Catalysts Crystallite Size

Catalyst crystallite size was determined by broadening of diffraction peaks using Scherrer's equation:

$$D = 0.9\lambda/(\beta - \beta_0)\cos\theta \qquad (4)$$

where, λ = wavelength of X-ray radiation (Mo $K_{\alpha 1}$ = 0.7093171 Å), β = breadth at half maximum intensity of a diffraction peak; β_0 = instrumental broadening of diffraction peaks; θ = Bragg angle.

Instrumental diffraction peak broadening was determined by measuring X-ray diffraction standard LaB_6.

Crystallite size represents the size of coherently diffracting domain and it cannot be always considered as particle size because of the presence of polycrystalline aggregates.

The powder X-ray diffraction pattern for Al_2O_3 mixed nickel catalysts (2:1 wt.%) (Figure 1a) shows the presence of alumina and nickel peaks. Few initial peaks of Al_2O_3 disappeared as prolonged ball milling was carried out leading to the amorphization of Al_2O_3. No oxidation of nickel was observed throughout the ball milling time. The calculated crystallite sizes for alumina mixed nickel ball milled for 1, 2 and 4 h are 184, 158 and 150 Å respectively.

X-ray diffraction pattern for Fe_3O_4 catalyst ball milled for different times are shown in Figure 1b. As the crystallite sizes decreased due to prolonged ball milling, diffraction peaks shift towards the low angle direction and peak widths increase. The crystallite size of coarser magnetite (in micron) decreased to 181 and 169 Å for 1 and 2 h ball milling time respectively.

Figure 1c depicts the X-ray diffraction pattern for variously ball milled Raney nickel. Peak width broadening can be observed for prolonged ball milling time. The crystallite sizes for raw, 2 and 4 h ball milled Raney nickel are 413, 209 and 190 Å respectively. Table 1 summarizes the crystallite sizes of all the variously ball milled catalysts.

During the prolonged milling time, the energy produced by ball milling drastically reduces the grain sizes and thus increases the lattice strain. It is a fact that the milling may cause several modifications such as vacancies [34]; atomic site interchanges [32] and dislocations [25]. Raney nickel is composed mainly of single element nickel and hence nullifies the effect of any atomic site interchanges for different ball milling time. Other modifications could be the formation of vacancies and dislocations in the unit cells of the catalysts powder particles. The developed lattice strain caused by mechanical milling is attributed to plastic deformation which is the generation and movement of dislocations [35,36]. According to Fecht [37], the generation and movement of dislocations could decrease grain size. High lattice strain implies to a high density of dislocation formation and which contributes to a reduction in grain size. If the grain size of catalysts particle decreases slowly that means there is a relatively less formation and movement of dislocations. Here, for both 2 h ball milled alumina mixed nickel and 2 h ball milled Raney nickel, there is a relatively higher % reduction in crystallite sizes. This suggests that the mechanical milling caused a severe plastic deformation to these catalysts powder particles.

Table 1. Crystallite size of variously ball milled catalysts.

Ball milling time (h)	Al$_2$O$_3$ Mixed nickel (Å)	Magnetite (Å)	Raney nickel (Å)
0	-	Micron size	413
1	184	181	-
2	158	169	209
4	150	-	190

Figure 1. XRD Pattern for variously ball milled (**a**) Al$_2$O$_3$: Ni (**b**) magnetite (**c**) Raney nickel.
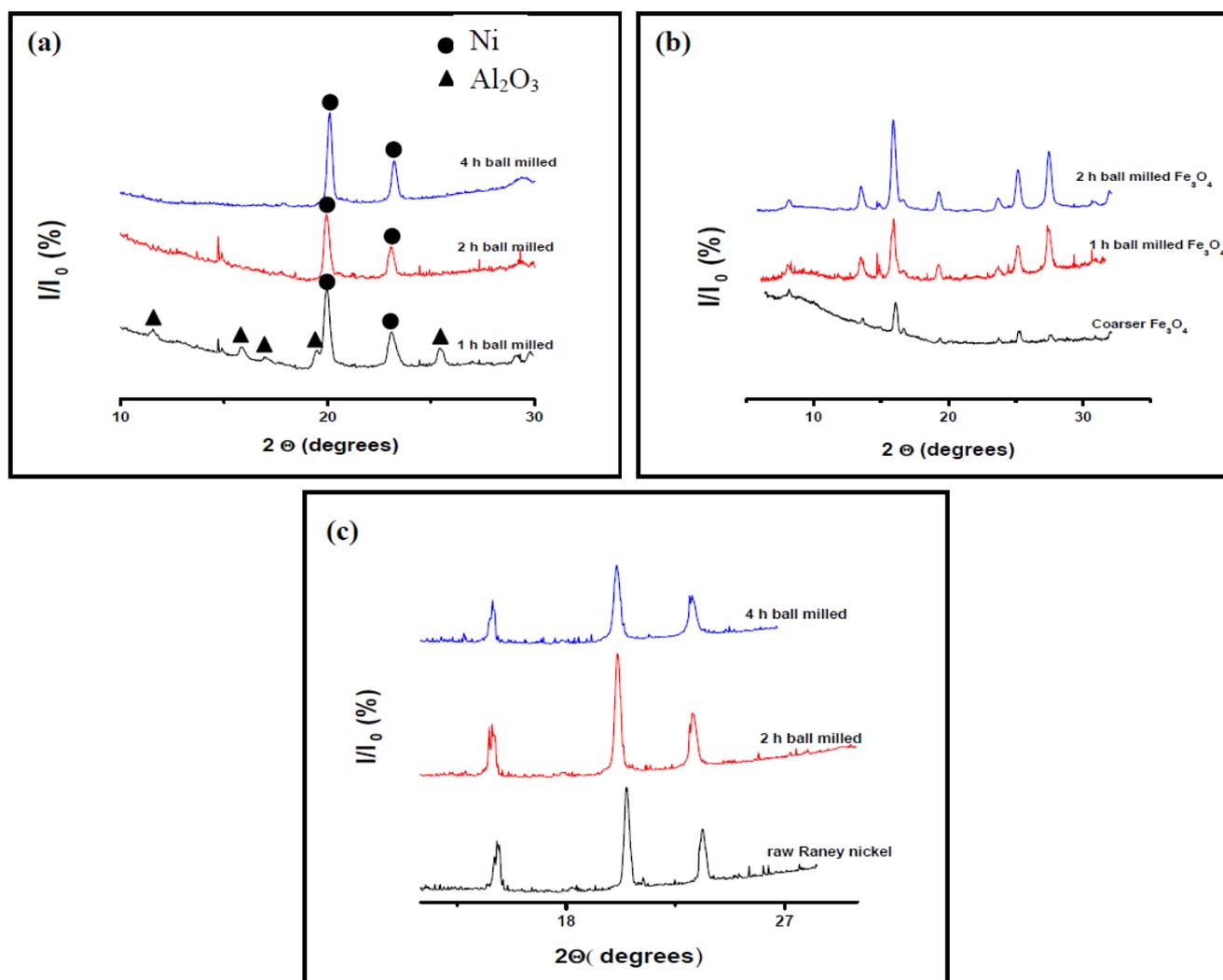
3.1.2. Morphology and Particle Size Analysis

Scanning electron microscope (SEM) was used to determine the surface morphology of the catalysts. Al$_2$O$_3$ mixed nickel ball milled for 2 h, shown in (Figure 2a), exhibits sponge- like morphology and consists of many small particles. The average particle sizes are 3.24, 3.26 and 2.80 µm for the milling time of 1, 2 and 4 h, respectively.

Figure 2b shows the surface morphology for variously ball milled magnetite catalyst particles. Coarse magnetite has relatively larger average particle size. The average particle sizes are 4.56, 3.09

and 2.62 μm for the milling time of 0, 1 and 2 h respectively. One should note that average particle size of magnetite decreases with increase in ball milling time.

Figure 2. SEM image of (**a**) alumina supported Nickel ball milled for (**i**) 1h. (**ii**) 2 h. (**iii**) 4 h and (**b**) Magnetite ball milled for (**i**) Without (**ii**) 1 h (**iii**) 2 h ball milling at 2000× each.
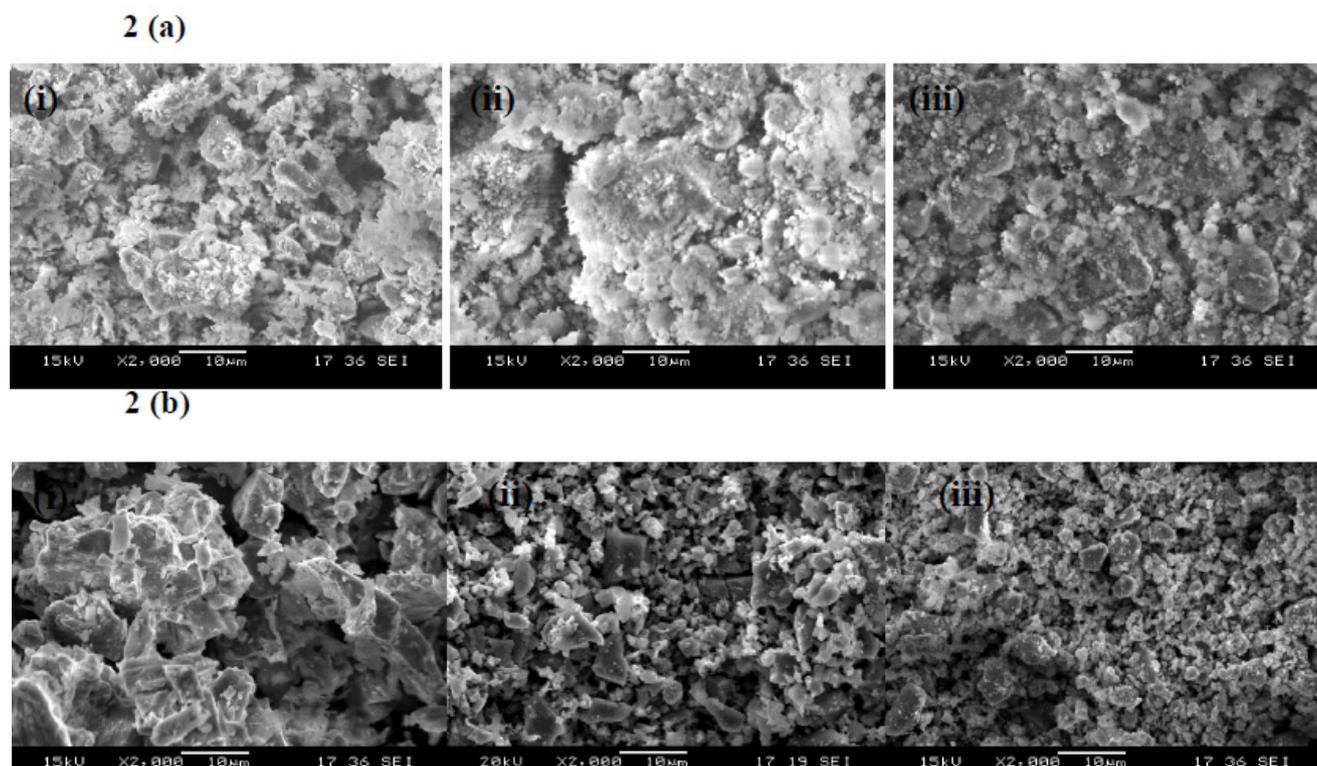
Figure 3 depicts the SEM images for variously ball milled Raney nickel. A relatively high number of openings or caves are observed for 2 h ball milled catalyst as shown in Figure 3iv. The globular particles of 2 h ball milled catalyst can be assumed to be a stacked layer of flaky disk particles (formed as an attrition product of raw Raney nickel). However, further attrition of these globular particles changed them back to platelet structure (Figure 3iii).

Moreover, the sizes of Raney nickel particles varied significantly over different ball milling periods. Initially, raw Raney nickel particles are almost spherical in shape and have a very wide distribution of the particle sizes. The average particle size of raw, 2 and 4 h ball milled Raney nickel are 11.74, 15.72, and 13.72 μm respectively.

It is well known that milling process is controlled by the two processes of cold welding and fracture [38,39]. Figure 4 illustrates the change in average particle size with milling time for variously ball milled catalysts. It also demonstrates the dominant stages of milling process with time for different catalysts. The particle size and morphology of catalysts are determined by the competition between cold welding and fracture process. The average particle sizes of Raney nickel increases until 2 h milling time which is attributed to the dominant cold welding process. However, fracture process dominates only after 2 h and causes a decrease in the average particle size for 4 h milling time. Al_2O_3 mixed nickel catalyst also shows the similar trends. Al_2O_3 mixed nickel has almost constant particle

size for first 2 h and then decrease in the average particle size was observed. It means that initially cold welding was dominant process and after 2 h milling time, it was the fracture process which prevailed. However, magnetite showed a different tendency for the milling process. The decrease in the magnetite average particle size with milling time is due to the dominant fracture process. It should be noted that for Al_2O_3 mixed nickel and Raney nickel, fracture process dominates only after 2 h milling time.

Figure 3. SEM image of Raney nickel (**i**) without; (**ii**) 2 h; (**iii**) 4 h ball milling at 2000× each and (**iv**) 2hball milled Raney nickel with pores (at 5000×).
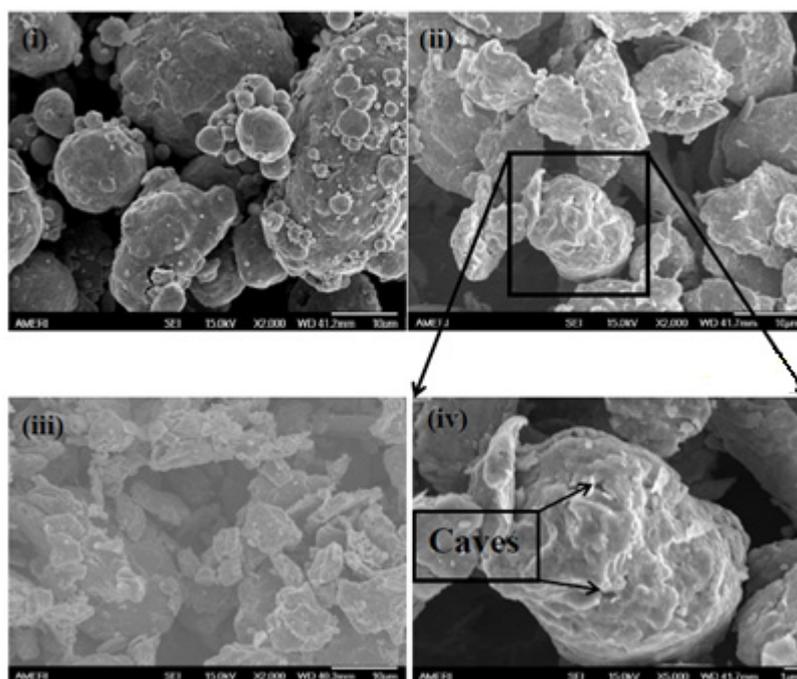
Figure 4. Change of average particle size of catalysts with milling time.
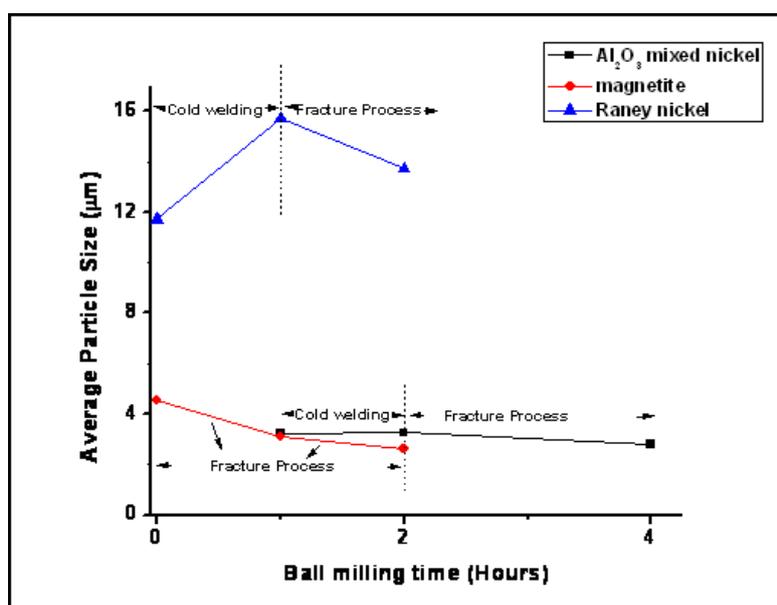
3.2. Reaction Results

The curves for % conversion of NaOH to Na_2CO_3 in the presence of variously ball milled Al_2O_3 mixed nickel, magnetite and Raney nickel catalysts at 300 °C are shown in Figures 5, 6 and 7 respectively. A substantial increase in the % conversion of NaOH to Na_2CO_3 was observed due to addition of the catalyst. However, a clear distinction between the catalytic activities for these catalysts becomes discernible only after a 30 min run (Figures 5–7). The obvious reason could be due to the formation of product Na_2CO_3, which once formed shows catalytic activity for the reaction [40].

Figure 5. % Conversion of NaOH to Na_2CO_3 for variously ball milled Al_2O_3: Ni (2:1) (wt.%) at 300 °C. 2 h ball milling time has exhibited the best result.
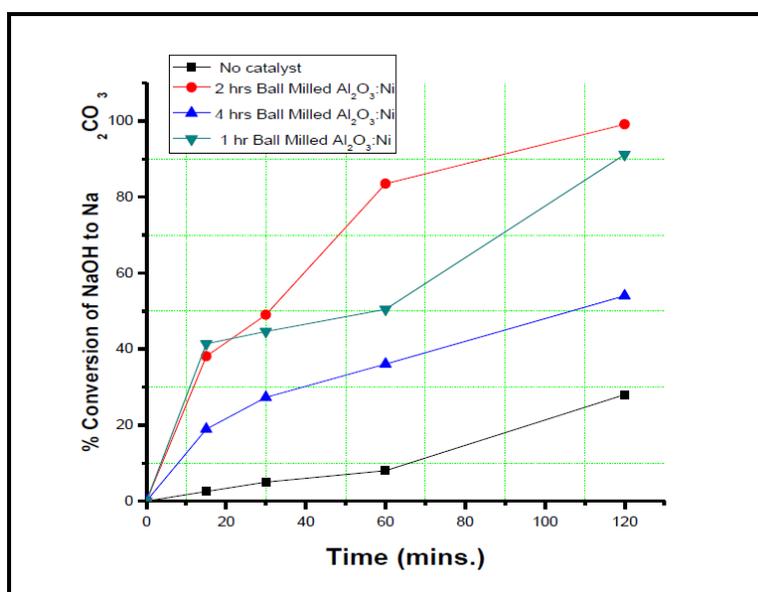
Figure 6. % Conversion of NaOH to Na_2CO_3 for variously ball milled Magnetite at 300 °C. 1 and 2 h Ball milling time has exhibited comparable result.
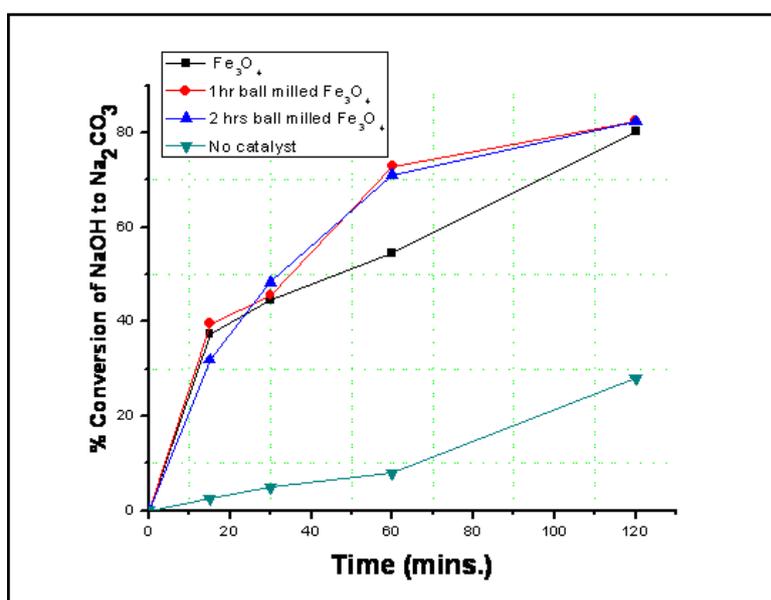
Figure 7. % Conversion of NaOH to Na$_2$CO$_3$ for Raney nickel at 300 °C. 2 h ball milling time has exhibited the best result.
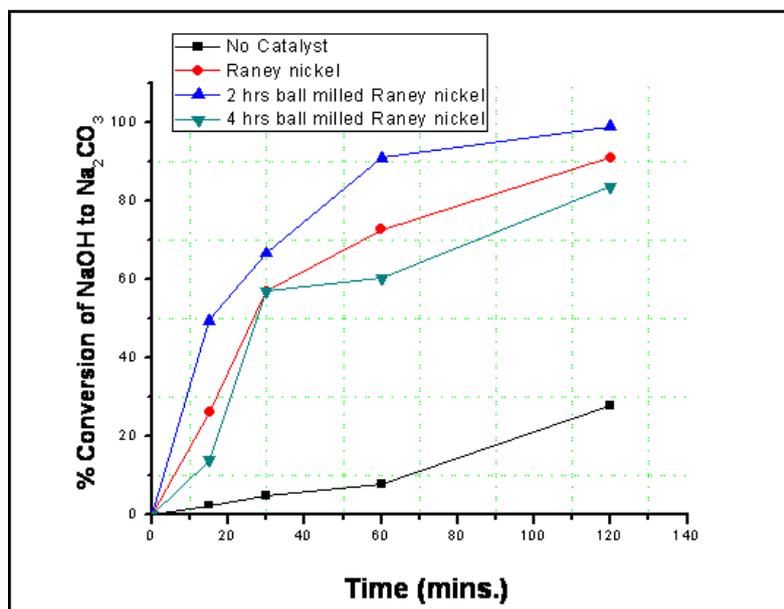
A 2 h ball milled Al$_2$O$_3$ mixed nickel catalyst was catalytically most effective compared to other Al$_2$O$_3$ mixed catalysts. The purpose to add Al$_2$O$_3$ with nickel was to avoid the chance of agglomeration. In our previous work [11], we observed that nickel particles tend to agglomerate when ball milled in the absence of dispersant (such as alumina) [11]. In this study, we have minimized the coalescence by mixing alumina with nickel. X-ray diffraction study (Figure 1a) confirms the amorphization of alumina over prolonged milling time. Smaller crystallite size for Al$_2$O$_3$ mixed nickel was generated as ball milling time was increased. Therefore, a better specific surface area and thus a better reaction yield were expected but the amorphization of alumina particles has caused the reverse effect. Therefore, the effective surface area available for the adsorption of the gas was decreased and hence a relatively lower reaction yield was observed. Higher mechanical attrition and thermally induced deactivation could be another major cause for low catalytic activity of 4 h alumina mixed nickel. It can also be observed that the maximum% reduction in crystallite size was observed for 2 h of ball milling time for alumina mixed nickel catalysts. Therefore, an increase in the formation and movement of dislocations or vacancies as well as exchange of atomic site positions have led to the increased catalytic activity for 2 h ball milled alumina mixed nickel catalysts.

In the experiments using magnetite as a catalyst, the reaction yield shows a similar reaction yield for 1 and 2 h milling time (Figure 6). Due to the larger crystallite size, coarser magnetite has a low surface area to volume ratio. The poor reaction yield in the presence of coarser magnetite was in consistent with its relative larger particle size. When magnetite was milled for 1 h, crystallite size reduced from several microns to 181 Å and that causes an increase in the catalytic activity. But for 2 h milling time, crystallite size reduced by only 12 Å compared to 1 h ball milled magnetite. Therefore, there is a relatively less plastic deformation for 2 h ball milled magnetite. Hence, 2 h ball milled exhibited identical catalytic activity to that of 1 h. Thus, it can be stated that the reaction yield goes hand in hand to the particle size of magnetite. 1 and 2 h ball milled magnetite has comparable crystallite size and therefore their reaction yields are also similar.

The effect for the use of Raney nickel catalyst on reaction (1) is illustrated in Figure 7. The curve shows that 2 h ball milled Raney nickel catalysts have the best results. 4 h ball milled Raney nickel catalysts have a low catalytic effect on reaction (1). The deactivation of 4 h ball milled Raney nickel can be due to either a high mechanical abrasion of the catalysts surface or thermally induced deactivation. The cold welding process dominates until 2 h of mechanical milling time for Raney nickel catalysts. As well as maximum % reduction in crystallite size was also observed for 2 h milling time only. Therefore, a large number of formations and movement of dislocations or vacancies have led to an increased catalytic activity for 2 h ball milled Raney nickel catalysts. However, there is a relatively less reduction in the crystallite size for 4 h milling time. Moreover, X-ray diffraction pattern for 4 h ball milling time clearly shows the amorphorization for the catalyst. Hence, 4 h milling time decreased the catalytic activity of Raney nickel.

Raw Raney nickel has a very wide distribution of particle sizes. Due to globular shape, they possess higher surface area. The globular particles are formed by the agglomeration of the disk-shaped particles by folding, enclosure, unfolding and pile-up [41]. Large number of open pores or caves formation allowed 2 h ball milled Raney nickel to show the highest catalytic activity compared to others. In summary, globular particles for Raney nickel has shown a better effect on reaction (1) compared to platelet like structure.

4. Conclusions

The exothermic reaction between NaOH and CO leads to the formation of Na_2CO_3 and H_2. This method of generating H_2 can be regarded as a carbon-free emission method. At 300 °C in the presence of 2 h ball milled alumina mixed nickel or Raney nickel catalyst, the reaction showed almost 100% conversion for a 120 min run. However, in the presence of 2 h ball milled Raney nickel, reaction (1) has highest % conversion of NaOH to Na_2CO_3 at any reaction time. In conclusion, 2 h ball milled globular Raney nickel has an overall best effect for NaOH-CO reaction. Moreover, particle size of the catalysts has an effect on the reaction yield. Longer milling causes a decrease in the catalytic activity for both alumina mixed nickel or Raney nickel catalysts. The equal crystallite size of 1 and 2 h ball milled magnetite has shown similar reaction yield.

References

1. Saxena, S.; Kumar, S.; Drozd, V.A. Modified steam-methane-reformation reaction for hydrogen production. *Int. J. Hydrog. Energy* **2011**, *36*, 4366–4369.
2. Saxena, S.K.; Drozd, V.; Durygin, A. A fossil-fuel based recipe for clean energy. *Int. J. Hydrog. Energy* **2008**, *33*, 3625–3631.
3. Reichman, B.; Mays, W.; Strebe, J.; Fetcenko, M. Ovonic Renewable Hydrogen (ORH—low temperature hydrogen from renewable fuels. *Int. J. Hydrog. Energy* **2010**, *35*, 4918–4924.
4. Kamo, T.; Takaoka, K.; Otomo, J.; Takahashi, H. Effect of steam and sodium hydroxide for the production of hydrogen on gasification of dehydrochlrinated poly (vinyl chloride). *Fuel* **2006**, *85*, 1052–1059.
5. Onwudili, J.A.; Williams, P.T. Role of sodium hydroxide in the production of hydrogen gas from the hydrothermal gasification of biomass. *Int. J. Hydrog. Energy* **2009**, *34*, 5645–5656.

6. Wang, H.Z.; Leung, D.Y.C.; Leung, M.K.H. A review on hydrogen production using aluminum and aluminum alloys. *Renew. Sustain. Energy Rev.* **2009**, *13*, 845–853.

7. Ahmad, S.; Aitani, A.; Rahman, F.; Al-Dawood, A.; Al-Muhaish, F. Decomposition of hydrocarbons to hydrogen and carbon. *Appl. Catal. A* **2009**, *359*, 1–24.

8. Muradov, N. Hydrogen via methane decomposition: An application for decarbonization of fossil fuels. *Int. J. Hydrog. Energy* **2001**, *26*, 1165–1175.

9. Drozd, V.; Saxena, S.K.; Garimella, S.V.; Durygin, A. Hydrogen release from a mixture of $NaBH_4$ and $Mg(OH)_2$. *Int. J. Hydrog. Energy* **2007**, *32*, 3370–3375.

10. Kalinci, Y.; Hepbasli, A.; Dincer, I. Biomass-based hydrogen production: A review and analysis. *Int. J. Hydrog. Energy* **2009**, *34*, 8799–8817.

11. Kumar, S.; Saxena, S.; Drozd, V.A. Modified method for production of Hydrogen from Methane. *Int. J. Energy Res.* **2012**, *36*, 1133–1138.

12. Muradova, N.Z.; Veziroglu, T.N. Green path from fossil-based to hydrogen economy: An overview of carbon-neutral technologies. *Int. J. Hydrog. Energy* **2008**, *33*, 6804–6839.

13. Ishida, M.; Otsuka, K.; Takenaka, S.; Yamanaka, I. One-step production of CO- and CO_2 -free hydrogen from biomass. *J. Chem. Tech. Biotech.* **2005**, *80*, 281–284.

14. Su, S.; Li, W.; Bai, Z.; Xiang, H.; Bai, J. Effects of ionic catalysis on hydrogen production by the steam gasification of cellulose. *Int. J. Hydrog. Energy* **2010**, *35*, 4459–4465.

15. Pistonesi, C.; Juan, A.; Irigoyen, B.; Amadeo, N. Theoretical and experimental study of methane steam reforming reactions over nickel catalyst. *Appl. Surface Sci.* **2007**, *253*, 4427–4437.

16. Matsumura, Y.; Nakamori, T. Steam reforming of methane over nickel catalysts at low reaction temperature. *Appl. Catal.* **2004**, *258*, 107–114.

17. Hou, K.; Hughes, R. The kinetics of methane steam reforming over a Ni/α-Al$_2$O catalyst. *Chem. Eng. J.* **2001**, *82*, 311–328.

18. Numaguchi, T.; Shoji, K.; Yoshida, S. Hydrogen effect on α-Al_2O_3 supported Ni catalyst for steam methane reforming reaction. *Appl. Catal. A* **1995**, *133*, 241–262.

19. Nozaki, T.; Muto, N.; Kado, S.; Okazaki, K. Dissociation of vibrationally excited methane on Ni catalyst Part 1. Application to methane steam reforming. *Catal. Today* **2004**, *89*, 57–65.

20. Hauptmann, H.; Walter, W.F. The action of raney nickel on organic sulfur compounds. *Chem. Rev.* **1962**, *62*, 347–404.

21. Gerhard, E.; Helmut, K. Bulk Catalysts and supports. *Prep. Solid Catal.* **1997**, *1*, 30–34.

22. Lund, C.R.F.; Kubsh, J.E.; Dumesic, J.A. Water-Gas Shift Over Magnetite-Based Catalysts: Nature of Active Sites for Adsorption and Catalysis. *ACS Symp. Ser.* **1985**, *279*, 313.

23. Rethwisch, D.G.; Phillips, J.; Chen, Y.; Hayden, T.F.; Dumesic, J.A. Water gas shift over magnetite particles supported on graphite: Effects of treatments in CO/CO_2 and H_2/H_2O gas mixtures. *J. Catal.* **1985**, *91*, 167–180.

24. Beeck, O. Catalysis and the Adsorption of Hydrogen on Metal Catalysts. *Adv. Catal.* **1950**, *2*, 151–195.

25. Trapnell, B.M.W. Specificity in catalysis by metals. *Quart. Rev.* **1954**, *8*, 404–421.

26. Gregg, S.J. *The Surface Chemistry of Solids*; Reinhold Pub. Corp.: New York, NY, USA, 1969; p. 233.

27. Beeck, O. Catalysis—A challenge to the Physicist. *Rev. Mod. Phys.* **1945**, *17*, 61–71.

28. Couper, A.; Eley, D.D. The parahydrogen conversion of palladium-gold alloys. *Discuss. Faraday Soc.* **1950**, *8*, 172–184.

29. Dowden, D.A.; Reynolds, P.W. Some reactions over alloy catalysts. *Discuss. Faraday Soc*. **1950**, *8*, 184–190.

30. Hofer, E.M.; Hintermann, H.E. Correlation between catalytic activity of Raney nickel and its structure. *Trans. Faraday Soc.* **1964**, *60*, 1457–1465.

31. Suryanarayan, C. Mechanical alloying and milling. *Prog. Mater. Sci.* **2001**, *46*, 1–184.

32. Koch, C.C. Synthesis of nanostructured materials by mechanical milling: Problems and opportunities. *Nanostruct. Mater.* **1997**, *9*, 13–22.

33. Guerrero-Paz, J.; Jaramillo-Vigueras, D. Nanometric grain formation in ductile powders by low energy ball milling. *Nanostruct. Mater.* **1999**, *11*, 1123–1132.

34. Zhou, L.Z.; Guo, J.T.; Jiang, T.D.; Wang, S.H. Investigation of defects in a mechanically alloyed nanocrystalline NiAl alloy by positron annihilation spectroscopy. *J. Mater. Sci. Lett.* **1998**, *17*, 137–139.

35. Liang, G.; Huot, J.; Schulz, R. Hydrogen storage properties of the mechanically alloyed LaNi5-based materials. *J. Alloys Compd.* **2001**, 320,133–139.

36. Mohamed, F.A. A dislocation model for the minimum grain size obtainable by milling. *Acta Mater.* **2003**, *51*, 4107–4119.

37. Fecht, H.J. Nanostructure formation by mechanical attrition. *Nanostruct. Mater.* **1995**, *6*, 33–42.

38. Zhou, J.B.; Rao, K.P. Structure and morphology evolution during mechanical alloying Ti-Al-Si powder systems. *J. Alloys Compd.* **2004**, *384*, 125–130.

39. Zhao, X.; Ding, Y.; Ma, L.; Shen, X.; Xu, S. Structure, morphology and electrocatalytic characteristics if nickel powders treated by mechanical milling. *Int. J. Hydrog. Energy* **2008**, *33*, 6351–6356.

40. Lee, S. *Alternative Fuels*; Taylors& Francis: Washington, DC, USA, 1996; p. 127.

41. Lee, G.G.; Hashimoto, H.; Watanabe, R. Development of Particle Morphology during Dry Ball Milling of Cu Powder. *Mater. Trans. JIM* **1995**, *36*, 548–554.